Key Words:
Hydrogen
Temperature
Membrane
Catalyst
Membrane Electrode Assembly

CLOSE-OUT REPORT FOR HYS ELECTROLYZER COMPONENT DEVELOPMENT WORK AT SAVANNAH RIVER NATIONAL LABORATORY

H. R. Colon-Mercado
M. Elvington
D. T. Hobbs

JANUARY 2010

Savannah River National Laboratory
Savannah River Nuclear Solutions
Aiken, SC 29808

Prepared for the U.S. Department of Energy Under Contract Number DE-AC09-08SR22470

SRNL SAVANNAH RIVER NATIONAL LABORATORY

DISCLAIMER

Printed in the United States of America

Prepared for
U.S. Department of Energy

Key Words:
Hydrogen
Temperature
Membrane
Catalyst
Membrane Electrode Assembly

CLOSE-OUT REPORT FOR HYS ELECTROLYZER COMPONENT DEVELOPMENT WORK AT SAVANNAH RIVER NATIONAL LABORATORY

H. R. Colon-Mercado
M. Elvington
D. T. Hobbs

JANUARY 2010

Savannah River National Laboratory
Savannah River Nuclear Solutions
Savannah River Site
Aiken, SC 29808

Prepared for the U.S. Department of Energy Under
Contract Number DE-AC09-08SR22470

SRNL SAVANNAH RIVER NATIONAL LABORATORY

TABLE OF CONTENTS

LIST OF FIGURES

LIST OF TABLES

LIST OF ACRONYMS

ATR	attenuated total reflectance
BPVE	perfluorocyclobutane-biphenyl vinyl ether
BPVE-6F	perfluorocyclobutane-biphenyl vinyl ether hexafluoroisopropylidene
CV	Cyclic Voltammogram
EIS	Electrochemical Impedance Spectroscopy (EIS)
EW	equivalent weight
FEP	fluorinated ethylene propylene
FTIR	Fourier transform infrared spectroscopy
GES	Giner Electrochemical Systems
HyS	hybrid sulfur
IR	infrared spectroscopy
LSV	linear sweep voltammetry
MEA	membrane electrode assembly
OCP	open circuit potential
PA	phosphoric acid
PBI	polybenzimidizole
PEM	proton exchange membrane
PFSA	perfluorinated sulfonic acid
S-PFCB	sulfonated perfluorocyclobutyl aromatic ether polymer
SDAPP	sulfonated Diels-Alder polyphenylenes
SDE	sulfur dioxide depolarized electrolyzer
SEM	Scanning electron microscope
SHE	standard hydrogen electrode
SNL	Sandia National Laboratory
SRNL	Savannah River National Laboratory

1.0 EXECUTIVE SUMMARY

The chemical stability, sulfur dioxide transport, ionic conductivity, and electrolyzer performance have been measured for several commercially available and experimental proton exchange membranes (PEMs) for use in a sulfur dioxide depolarized electrolyzer (SDE). The SDE's function is to produce hydrogen by using the Hybrid Sulfur (HyS) Process, a sulfur based electrochemical/thermochemical hybrid cycle. Membrane stability was evaluated using a screening process where each candidate PEM was heated at 80 °C in 63.5 wt. % H_2SO_4 for 24 hours. Following acid exposure, chemical stability for each membrane was evaluated by FTIR using the ATR sampling technique. Membrane SO_2 transport was evaluated using a two-chamber permeation cell. SO_2 was introduced into one chamber whereupon SO_2 transported across the membrane into the other chamber and oxidized to H_2SO_4 at an anode positioned immediately adjacent to the membrane. The resulting current was used to determine the SO_2 flux and SO_2 transport. Additionally, membrane electrode assemblies (MEAs) were prepared from candidate membranes to evaluate ionic conductivity and selectivity (ionic conductivity vs. SO_2 transport) which can serve as a tool for selecting membranes. MEAs were also performance tested in a HyS electrolyzer measuring current density versus a constant cell voltage (1V, 80 °C in SO_2 saturated 30 wt% H_2SO_4). Finally, candidate membranes were evaluated considering all measured parameters including SO_2 flux, SO_2 transport, ionic conductivity, HyS electrolyzer performance, and membrane stability. Candidate membranes included both PFSA and non-PFSA polymers and polymer blends of which the non-PFSA polymers, BPVE-6F and PBI, showed the best selectivity.

Testing examined the activity for the sulfur dioxide oxidation of platinum base electrocatalyst in 30 wt% sulfuric acid solution. Linear sweep voltammetry showed an increase in activity when catalysts in which Pt is alloyed with non-noble transition metals such as cobalt, chromium and iron. However when Pt is alloyed with noble metals, such as iridium or ruthenium, the kinetic activity as well as the stability decreases.

2.0 INTRODUCTION

Continually increasing energy demands coupled with reliance on a diminishing supply of nonrenewable fossil fuels provides the impetus for innovative research into alternative energy generation and storage systems. One possible solution is centered on the energy carrier hydrogen, which contains the highest energy per mass ratio of any conventional fuel. Global scale quantities of hydrogen will be required for the ensuing economic transformation and major efforts are underway worldwide to develop the technologies required for this transition. These demands can be met by water electrolysis or through thermochemical water splitting cycles. Water electrolysis offers several advantages over other production methods [1], however, the technology required and energy input can make hydrogen produced by this method expensive. Thermochemical water splitting cycles offer an alternative highly efficient route for hydrogen production [2]. Among the many possible thermochemical cycles for the production of hydrogen, the sulfur-based cycles lead the competition in overall energy efficiency.

The Hybrid Sulfur (HyS) Process is a sulfur-based thermochemical cycle containing a low energy electrolysis step making it a thermo/electrochemical hybrid process. In this process sulfuric acid is thermally decomposed at high temperature (> 800 °C) producing SO_2 [r1]. H_2SO_4 saturated with SO_2 is then pumped into a sulfur dioxide-depolarized electrolyzer (SDE). The SDE electrochemically oxidizes sulfur dioxide to form sulfuric acid at the anode [r2] and reduces protons to form hydrogen at the cathode [r3]. The overall electrochemical reaction consists of the production of H_2SO_4 and H_2 [r4], while the entire cycle produces H_2 and O_2 from H_2O with no side products [r5].

$$H_2SO_4 \rightarrow SO_2 + \tfrac{1}{2}O_2 + H_2O \quad [r1]$$

$$SO_2 + 2H_2O \rightarrow H_2SO_4 + 2H^+ + 2e^- \quad [r2]$$

$$2H^+ + 2e^- \rightarrow H_2 \quad [r3]$$

$$SO_2 + 2H_2O \rightarrow H_2SO_4 + H_2 \quad [r4]$$

$$2H_2O \rightarrow 2H_2 + O_2 \quad [r5]$$

HyS electrolysis (SO_2 oxidation) [r2] has a reversible half cell potential of -0.158 V (SHE) [3], while low temperature water electrolysis has a reversible half cell potential of -1.23 V (SHE). Thus, the HyS process requires much less electrical energy input than water electrolysis. Due to ohmic, kinetic, and mass transport overpotential losses, an operating potential of 0.6 V has been targeted for the HyS electrolyzer at a current density of 500 mA cm^{-2}.

Development of the SDE began in the late 1970s utilizing a parallel-plate electrolyzer with a separator/membrane to keep the anolyte and catholyte compartments separate [4]. Since this work in the early 1980s, significant advances have occurred in electrolyzer technology principally in the area of hydrogen fuel cells. Advanced hydrogen fuel cells employ proton conductive membranes with catalyst layers deposited on both sides of the membrane, forming the respective anode and cathode of the electrochemical cell. The layered structure containing membrane and electrode catalysts is referred to as the MEA. Upon resumption of HyS work in 2005, the fuel cell MEA design concept was applied to the SDE [5,6]. The MEA concept results in a much smaller cell footprint than conventional parallel plate technology, which is a major benefit when implementing the SDE on a commercial scale.

There are several requirements of a PEM for the successful functioning of a HyS electrolyzer. The PEM must be stable in highly corrosive solution (>30 wt% H_2SO_4 saturated with SO_2) and at high operating temperature (>80 °C), allow minimal transport of SO_2, and must maintain high ionic conductivity. Ideally, operating temperatures well above 80° C are desired with acid concentrations greater than 50 wt% H_2SO_4. These conditions allow the electrolyzer to function at low cell potential and high current density thus minimizing the energy input and maximizing hydrogen output. Lastly, the PEM serves to separate the anolyte reagents from the hydrogen output to prevent the production of undesired sulfur-based side reaction products and poisoning of the cathode catalyst.

3.0 EXPERIMENTAL

3.1 MEMBRANE PROCUREMENT AND PREPARATION

The selection process of commercially available and experimental membranes took into account: thickness, equivalent weight (EW), conductivity, chemical stability, and permeability to uncharged molecules. Prior to testing, all membranes were hydrated by immersing in deionized water for several minutes. Commercial membranes included perfluorinated sulfonic acid (PFSA) membranes [7] from DuPont and polybenzimidizole (PBI) [8] membranes from BASF, Figure 1. Experimental membranes were synthesized with the primary objective of reducing the transport of neutral charge species such as dissolved SO_2. These membranes included hydrated, sulfonated Diels-Alder polyphenylenes (SDAPP) [9] from Sandia National Laboratory (SNL); stretched recast Nafion® and PFSA/fluorinated ethylene propylene (FEP) blends from Case Western Reserve University; hydrated treated Nafion® 115 from Giner Electrochemical Systems (GES); and perfluorocyclobutane-biphenyl vinyl ether (BPVE) and perfluorocyclobutane-biphenyl vinyl ether hexafluoroisopropylidene (BPVE-6F) polymer blends from Clemson University (Figure 1) [10].

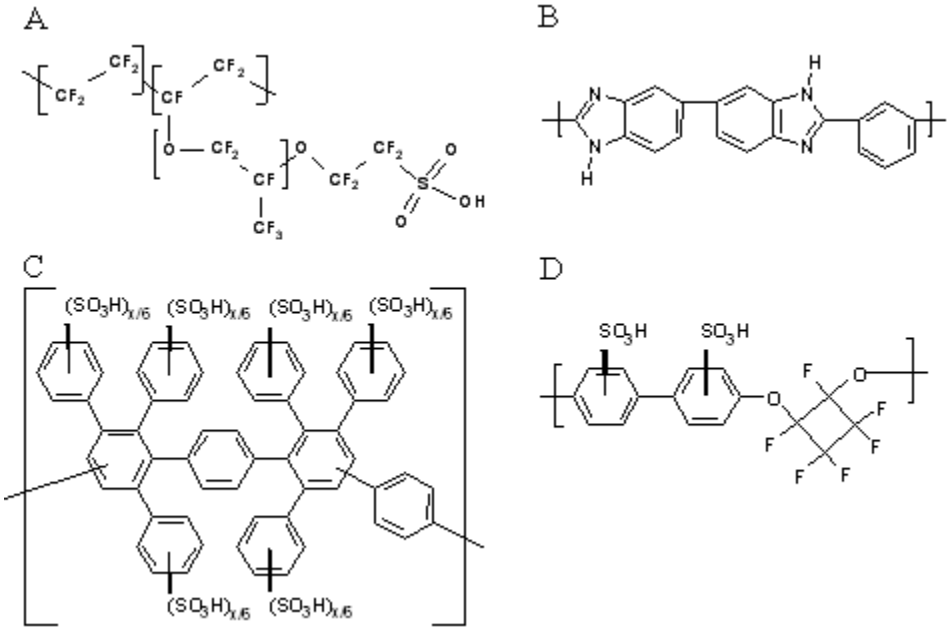

Figure 1. Evaluated commercial and experimental membranes including a.) perfluorinated sulfonic acid, b.) polybenzimidizole, c.) sulfonated Diels-Alder polyphenylenes, and d.) perfluorocyclobutane-biphenyl vinyl ether hexafluoroisopropylidene.

3.2 MEMBRANE CHEMICAL STABILITY MEASUREMENT

The chemical stability of the membranes in a corrosive environment was examined using a screening method to provide insight into the potential long-term performance. All membranes were exposed to 9.2 molar (63.5 wt%) H_2SO_4 at 80 °C for 24 hours. Following acid exposure, the membranes were rinsed and stored in deionized water until analysis. Fourier transform infrared spectroscopy (FTIR) was used with the attenuated total reflectance (ATR) sampling technique. IR spectra taken before and after acid exposure were compared to determine impact on membrane functional groups. FTIR spectra were measured with a Jasco FT/IR-6300 instrument before and after exposure to sulfuric acid solution.

3.3 MEMBRANE SO_2 TRANSPORT MEASUREMENT

Membrane transport of SO_2 was evaluated under non-polarized conditions using a permeation cell designed and fabricated at Savannah River National Laboratory (SRNL); a schematic of the cell is shown in Figure 2. The cell consists of two glass chambers joined by a Teflon™ bridge where the membrane is secured. The bridge consists of a diffusion layer in the left chamber where acid saturated with SO_2 is forced by pump A into the anolyte-membrane interface. Additionally, the diffusion layer presses the membrane to the working electrode, which is supported by a perforated tantalum plate that provides electrical connection to the working electrode. Finally, a non-conductive diffusion media separates the tantalum support from the counter electrode in order to allow the flow of fresh acid pumped by pump B to the counter electrode without short circuiting the cell.

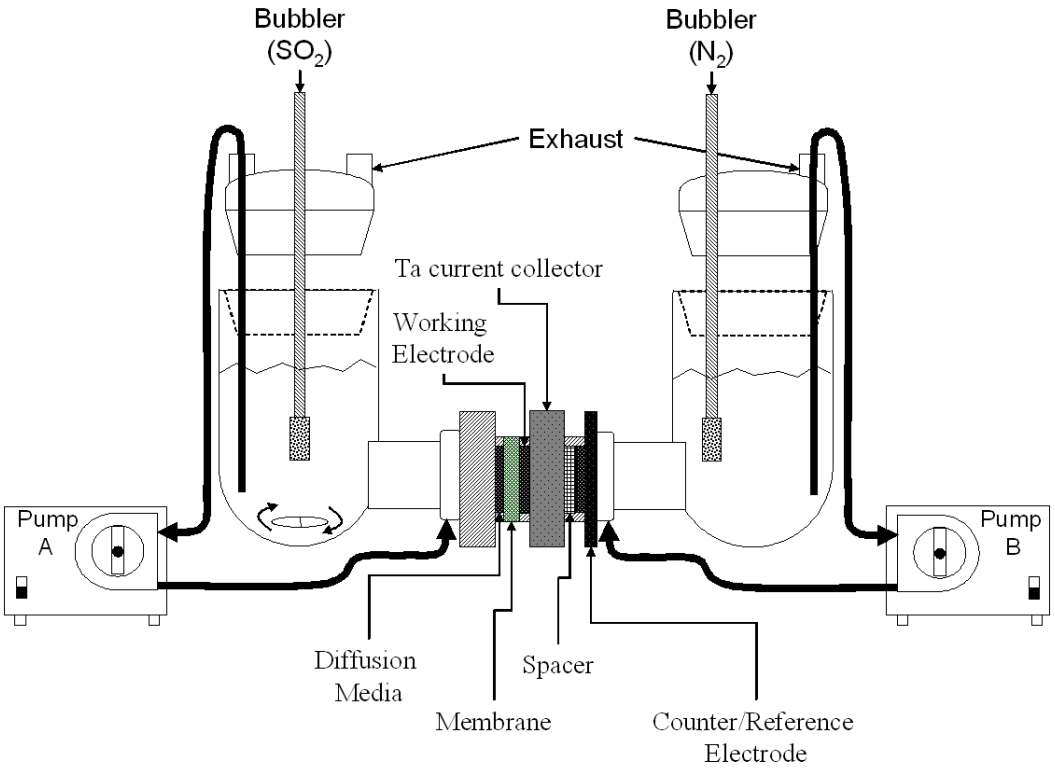

Figure 2. Simplified schematic of the SO_2 transport characterization cell consisting of two glass chambers joined by a Teflon bridge which houses the membrane, working electrode, and counter/reference electrode.

During measurements both chambers were filled with 30 wt% sulfuric acid and purged of oxygen by flowing nitrogen. A two-electrode system consisting of a platinum mesh working electrode and a porous carbon counter electrode was used during measurements. SO_2 transport was determined by measuring the current as a function of time while a constant potential of 1.2 V was applied using a PARSTAT 2273 electrochemical analyzer. Once the background current stabilized close to zero, SO_2 was introduced into the cell within the left chamber by bubbling. SO_2 permeating through the membrane was oxidized to sulfuric acid by the working electrode. The permeation current increased with time until steady-state conditions are reached and no change in flux is observed. SO_2 transport was measured for a period of one hour and then analyzed. If the current did not reach a steady state within the first hour, the experiment was continued for an additional hour and then reassessed. The time required to reach steady state is mostly dependent on the equilibration time between the membrane and the liquid electrolyte. Assuming all the SO_2 transported was

electrochemically oxidized, the SO_2 flux, J_{SO_2}, can be calculated from the current response using Faraday's Law,

$$J_{SO_2} = \frac{i}{nF} \qquad \text{[eq1]}$$

where i is the current density in A cm^{-2}, F is Faraday's constant (96,487 C/eq.), and n is the number of electrons transferred assuming [r2]. Nafion® 115 and Nafion® 211 were used as baselines for all SO_2 flux and SO_2 transport measurements. A plot of SO_2 flux over time for the two baseline materials is shown as an example, Figure 3.

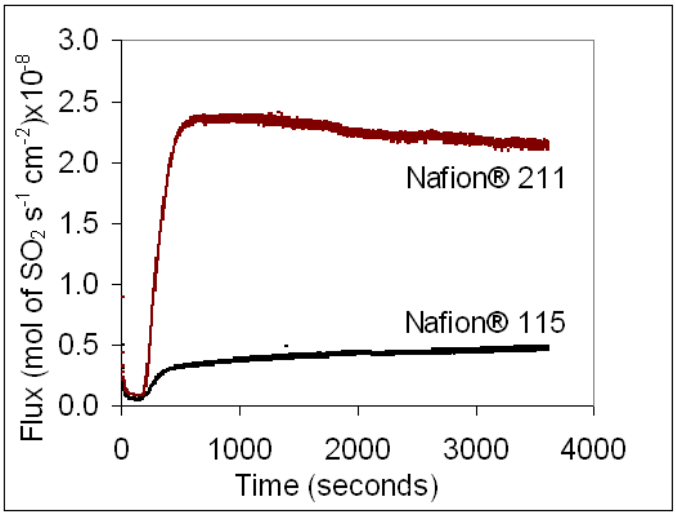

Figure 3. Measured SO_2 flux for Nafion® 115 and Nafion® 211.

The solubility of SO_2 within the membranes is unknown so D, the SO_2 diffusion coefficient, cannot be determined. SO_2 transport can, however, be estimated from Fick's first law of diffusion by substituting the solubility of dissolved SO_2 in the membrane for the bulk SO_2 concentration,

$$SO_2 \text{ transport} = \frac{J_{SO_2} L}{C_0} \qquad \text{[eq2]}$$

where J_{SO_2} is the SO_2 flux, L is the thickness of the membrane, and C_0 is the bulk concentration of SO_2 (estimated to be 1.09 M in 30 wt% H_2SO_4 and 0.952 M in 50 wt% H_2SO_4)[3].

3.4 IONIC CONDUCTIVITY MEASUREMENT

The ionic conductivity of each membrane was measured as was the performance in a HyS electrolyzer cell. Membrane Electrode Assemblies (MEAs) were prepared in order to measure these properties. A Paasche Millennium double action airbrush was used for MEA preparation to apply the catalyst "ink" via the spray-deposition technique. Typical catalyst layers consist of 25 wt% Nafion® ionomer as a binder, and 75 wt% platinized carbon (TKK; 45.9 wt% Pt). Anode and cathode catalyst layers were targeted at 1.8 mg Pt cm^{-2} and 0.9 mg Pt cm^{-2} respectively. A PARSTAT 2273 potentiostat (Princeton Applied Research) was used for all electrochemical measurements.

Electrochemical Impedance Spectroscopy (EIS) was used to evaluate the ionic resistivity (ρ) for each membrane. For this measurement MEAs were used in a HyS electrolyzer cell to minimize the contact resistance. After allowing the membrane to equilibrate for several minutes, a 10 mV vs. OCP (open circuit potential) sinusoidal voltage was applied across the membrane at frequencies ranging from 500 kHz to 200 Hz. The resulting response was displayed in the form of a Nyquist plot. The resistance was calculated from the value of the real impedance when the imaginary response was zero. The ionic conductivity, λ, was calculated using the following equation,

$$\lambda = \frac{L}{Z_{real} A} \qquad \text{[eq3]}$$

where L is the thickness of the membrane, A is the area available for proton conduction, and Z_{real} is the real part of the impedance response when the imaginary impedance is zero.

3.5 ELECTROLYZER PERFORMANCE

Electrolyzer performance was evaluated in a HyS cell by applying a potential of 1 V across the MEA and measuring the current density over time. The anodic chamber contained 30 wt% H_2SO_4 saturated with SO_2 while the cathodic chamber contained deionized water. Prior to electrolysis both chambers were purged of oxygen by flowing argon. A potential of 1 V was then applied. Once the background current stabilized close to zero, SO_2 was introduced into the anolyte by bubbling and the resulting current due to SO_2 oxidation was measured.

3.6 ELECTROCATALYST ACTIVITY MEASUREMENT

The cell consisted of a glass vial with two compartments covered with a Teflon™ cap and separated with a fine glass frit. The three electrodes, which included a silver-silver chloride reference electrode, a platinum wire as the counter electrode, and a glassy carbon disk electrode (GCE), were inserted through the Teflon™ cap. The counter electrode was inserted in the second compartment to prevent reduction products from affecting the working electrode. The counter electrode compartment was purged with N_2 at all times. Figure 4 shows the simplified schematic of the catalyst characterization cell. To load the catalyst onto the GCE, a catalyst ink was prepared by ultrasonically blending the catalyst (2 mg) with 1mL of deionized, distilled water for 15 min in an ultrasonic bath. The ink (8 μL) was then placed on the GCE surface. After drying, a volume of ~2 μL of a mixture 1:20 of Nafion® solution (5 wt% from Aldrich) and methyl alcohol (Sigma) was applied on the dry catalyst to ensure adhesion on the GCE surface. Electrochemical characterization of each catalyst material featured cyclic voltammetry (CV) which was obtained using a PARSTAT 2273 electrochemical analyzer. Sulfuric acid solutions were prepared by diluting reagent grade sulfuric acid (Fisher Scientific) with deionized, distilled water. Prior to the measurements all solutions were purged of oxygen by bubbling nitrogen.

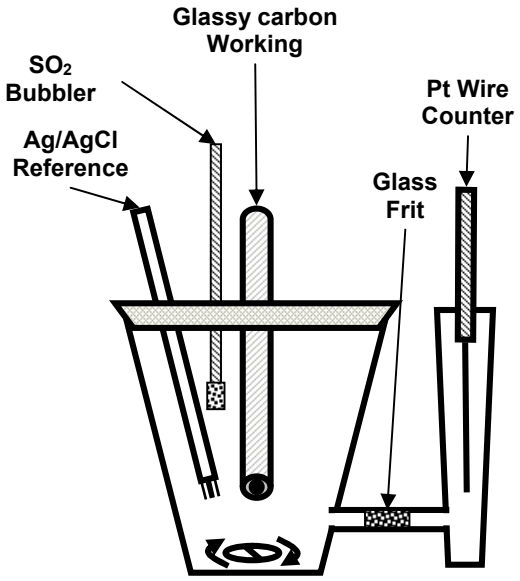

Figure 4. Simplified schematic of the catalyst characterization cell.

CVs were performed at a scan rate of 100 mV/sec and in a potential window between 1200 mV and -200 mV vs. Ag/AgCl. The experiments were carried out at a temperature of 25 ºC and a sulfuric acid concentration of 30 wt%. The curves were repeated until a stable performance was obtained. CV measurement was performed starting from the anodic potential and going in the cathodic direction.

Linear sweep voltammetry (LSV) was performed to establish the equilibrium potential for sulfur dioxide oxidation using a window of 0.604 V to 0.204 V (vs Ag/AgCl). The Ag/AgCl reference electrode was calibrated versus ferrocene throughout the course of experimentation to ensure no potential drift occurred due to contamination of the reference electrode. LSVs measuring SO_2 oxidation potentials were taken at room temperature in 30 wt.% H_2SO_4 saturated with SO_2 by bubbling.

4.0 DISCUSSION

4.1 MEMBRANE DURABILITY

The chemical stability of the membranes in a corrosive environment was examined to provide insight into the potential long-term performance. FTIR spectra taken before and after acid exposure were compared to determine impact on membrane functional groups. It was found that all PFSA type membranes suffered no measurable degradation when exposed to 63.5 wt% H_2SO_4 for 24 hours at 80° C. Also, no degradation was observed for SDAPP and S-PFCB samples. A spectral shift was observed in the 800 to 1200 cm^{-1} region for the PBI membrane, Celtec V, which corresponds to vibrations attributed to the doped acid anions, Figure 5 [11]. This small shift to higher wave numbers possibly indicates loss of H_3PO_4 from the membrane along with uptake of H_2SO_4. It has been previously shown that a H_2SO_4 doped PBI membrane has comparable conductivity, depending on doping level, to a H_3PO_4 doped membrane [11,12]. The high electrolyzer performance, both initially and after multiple hours of electrolysis, also suggests that if H_3PO_4 / H_2SO_4 exchange is occurring, no detrimental impact is apparent. No other spectral shifts are observed for the PBI membrane indicating the polymer backbone is intact

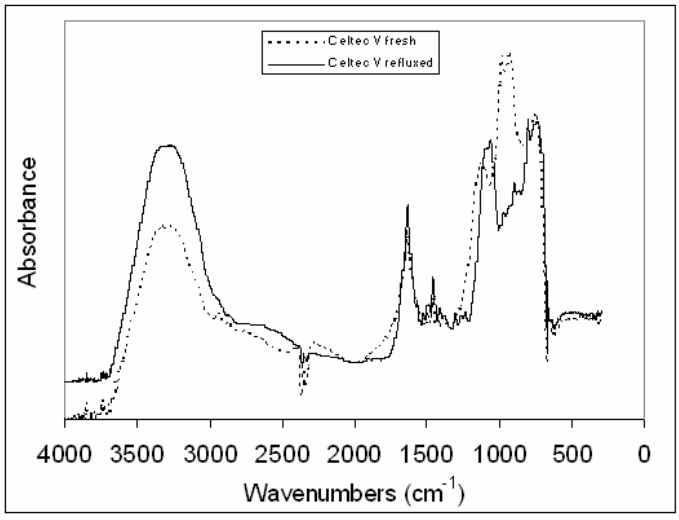

Figure 5. FTIR spectrum for PBI membrane Celtec V before (dotted line) and after (solid line) heating at reflux in 60 wt% H_2SO_4 at 80 °C for 24 hours.

4.2 MEMBRANE TRANSPORT OF SO_2 AND ELECTROLYZER PERFORMANCE

SO_2 flux, and SO_2 transport were determined for several commercially available and experimental membranes and tabulated along with membrane thickness in Table 1. Nafion®

115, equivalent weight (EW) 1100, is utilized in current HyS electrolyzer testing and, therefore, serves as a baseline for this work.

Table 1. SO_2 flux, SO_2 transport, conductivity, and current density (performance in HyS electrolyzer) is shown along with membrane thickness for a number of commercially available and experimental membranes.

Manufacturer and ID	Membrane Classification	Thickness (μm)	SO_2 Flux (mol SO_2 s^{-1} cm^{-2}) x 10^{-9}	SO_2 Transport (cm^2 s^{-1}) x10^{-8}	Conductivity (S cm^{-1})	Current Density (mA cm^{-2})
Dupont Nafion® 115	PFSA	127	5.23	6.10	0.0241	270
Dupont Nafion® 211	PFSA	25	21.8	5.09	0.0159	393
Dupont Bi-layer	Perflourinated Carboxyl/Sulfonic Acid	140	0.11	0.14	a	0.010
Dupont 1500EW	1500EW PFSA	100	0.14	0.13	a	0.005
Dupont 112/pvp46	Treated PFSA	50	6.61	3.08	0.0036	128
Dupont 1135/pvp48	Treated PFSA	90	6.01	4.90	0.0064	123
GES 672-90-1	Treated PFSA	127	12.6	14.7		
GES 672-90-2	Treated PFSA	127	10.2	11.9		
Case 1	Stretched PFSA	55	10.5	5.28		
Case 4	Stretched PFSA	63	19.8	11.7		
Case 60-40-2	PFSA-FEP blend	62	5.88	3.35		
Case 50-50-2	PFSA-FEP blend	55	5.96	3.01	0.0034	155
Case 45-55-2	PFSA-FEP blend	53	4.09	1.99	0.0096	228
Sandia SDAPP5192C	SDAPP	50-85	11.1	7.79	0.0328	286
Clemson B(2)	BPVE	18	21.2	3.50	0.0048	320
Clemson B1F1(1)	BPVE-6F (1:1)	16	16.2	2.37	0.0063	337
Clemson B2F1(3)	BPVE-6F (2:1)	19	17.6	3.07	0.0109	335
BASF Celtec-V	PBI	100	2.14	1.99		344

a. conductivity was to low to measure.

PFSA membranes, developed for low temperature (80 °C) PEM fuel cells, are known to have good chemical stability and conductivity, and have shown good performance in a HyS electrolyzer, see Figure 6. However, SO_2 transport is unacceptably high, leading to the formation of sulfur containing impurities at the cathode and ultimately reduced operational lifetime.

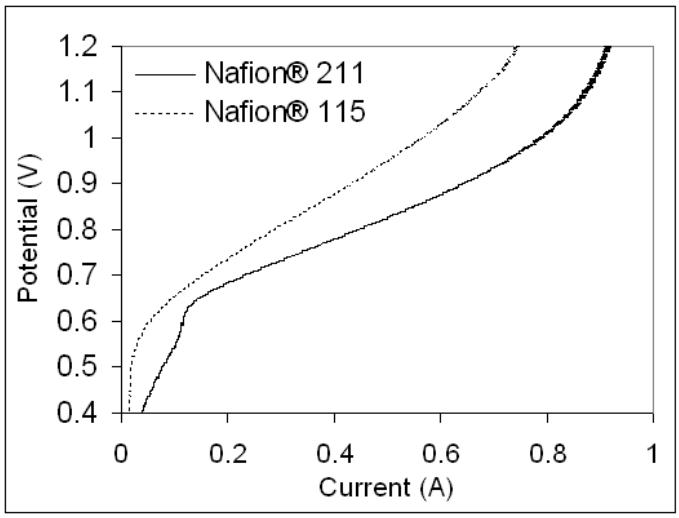

Figure 6. Polarization Curve for Nafion® 115 and Nafion® 211.

A number of PFSA-type membranes were prepared to reduce the transport of small neutral molecules such as SO_2 including: a bilayer of polyfluorinated carboxyl and sulfonic acid, Nafion® 1500 EW, and two treated Nafion® membranes from Dupont; two treated PFSA membranes from GES; and stretched recast PFSA membranes, and PFSA-FEP blends from Case Western Reserve University. Of the PFSA family of membranes, untreated Nafion® had the highest through-plane conductivity (0.0241 S cm^{-1}) and showed the best performance (270 mA cm^{-2}), while having mediocre SO_2 transport (6.10 x 10^{-8} cm^2 s^{-1}). Standard deviations for SO_2 flux and SO_2 transport measurements were typically less than 10% while standard deviations for electrolyzer performance was typically less than 2%. The 1500 EW Nafion® and the Nafion® bilayer had by far the lowest conductivity and performance but also had by far the lowest SO_2 flux and SO_2 transport of any membrane tested. Case 45-55-2, a PFSA-FEP blend, showed promise, having significantly lower SO_2 transport (1.99 x 10^{-8} cm^2 s^{-1}) than the baseline Nafion® 115 (6.10 x 10^{-8} cm^2 s^{-1}) while having only a small decrease in performance (228 mA cm^{-2} vs. 270 mA cm^{-2}). In general it was noted that most PFSA-type samples that had higher conductivities and electrolyzer performance also had higher SO_2 transport, while most samples that had low SO_2 transport also had low conductivity and exhibited poorer electrolyzer performance.

Non PFSA-type membranes were also tested including SDAPP, S-PFCBs, and PBI. SDAPP membranes were originally developed as a low cost alternative to PFSA with improved thermal stability while maintaining good chemical stability, ionic conductivity, and barrier properties to small neutral molecules. Sulfonation of Diels-Alder polyphenylenes results in a membrane that has excellent proton conductivity (0.0328 S cm^{-1}). SDAPP membranes employ the same proton conduction mechanism as PFSA, where sulfonic acid groups generate water channels inside the membrane which solvate and transport protons [7]. The SDAPP membrane performed well in the HyS electrolyzer (286 mA cm^{-2}), slightly higher than Nafion® 115 (270 mA cm^{-2}), however the SO_2 transport was similarly increased (7.79 x 10^{-8} cm^2 s^{-1} vs. 6.10 x 10^{-8} cm^2 s^{-1}). Thermal gravimetric analysis indicates SDAPP stability of up to 285 °C where SO_3 cleavage initiates, while DSC indicates a T_g well above the decomposition temperature [9]. Future testing will take advantage of this increased thermal stability which is expected to increase HyS electrolyzer performance by decreasing the kinetic overpotential.

Sulfonated perfluorocyclobutyl aromatic ether polymer (S-PFCBs) electrolytes were initially developed by Smith and co-workers at Clemson and Tetramer Technologies, LLC, for automotive PEM fuel cells [13,14]. Currently a variety of PFCB polymers and copolymers are under development, including BPVE and BPVE-6F, which are designed specifically for use in a HyS electrolyzer cell with the primary goal of suppressing SO_2 transport. The BPVE membrane, B(2), and BPVE-6F membranes, B1F1(1), and B2F1(3), all displayed high SO_2 flux (21.2, 16.2, and 17.6 mol SO_2 s^{-1} cm^{-2} respectively), however this is mostly a function of their relative thickness, all of which are less than 25 μm (1 mil). The SO_2 transport, which takes the membrane thickness into account, was found to be significantly lower than the baseline material (6.10 x 10^{-8} cm^2 s^{-1}) in all 3 membranes (B(2) = 3.50, B1F1(1) = 2.37, and B2F1(3) = 3.07 x 10^{-8} cm^2 s^{-1}) while displaying increased electrolyzer performance (320, 337, and 335 mA cm^{-2} respectively). A comparison to a PFSA membrane of similar thickness like Nafion® 211, however, may be more appropriate. All three BPVE membranes now show reduced SO_2 flux despite being thinner still, and lower SO_2 transport, while their conductivity and electrolyzer performance are somewhat lower than the excellent performance from Nafion® 211 (393 mA cm^{-2}). BPVE-6F (1:1) showed the best combination

of SO_2 transport, conductivity, and performance and will undergo further testing and development.

The PBI family of membranes were originally developed for Phosphoric Acid (PA) fuel cells and are known for their ability to operate at elevated temperatures and without humidification [15,16]. Unlike sulfonated membranes (PFSA, SDAPP, BPVE), that employ sulfonic acid groups to transport hydrated protons, PBI membranes employ a hopping mechanism in which immobilized anions, such as PA, can solvate protons whereby providing a path for rapid proton exchange. As a result, protons are conducted without the need of water channels. This can greatly reduce the transport of small neutral molecules, which is reflected in both the measured SO_2 flux (2.14×10^{-9} mol SO_2 s^{-1} cm^{-2}) and SO_2 transport (1.99×10^{-8} cm^2 s^{-1}), both of which are significantly lower than the baseline membrane. Amazingly, the HyS electrolyzer performance was also increased relative to the baseline (344 mA cm^{-2} vs. 270 mA cm^{-2}) indicating an effective proton exchange mechanism despite the decreased SO_2 transport. This combination of significantly improved performance and reduction of SO_2 transport make the PBI family of membranes a promising alternative demanding further study.

4.3 ELECTROCATALYST STABILITY

Consecutive CVs were performed to study the stability of the catalyst and the different electrochemical reactions occurring at the surface of the electrode in the absence of SO_2. During the CVs, the current was monitored as a function of a set potential which is varied at a constant rate. Figure 7 shows the typical consecutive CVs for Ru/C measured at room temperature in 30 wt% H_2SO_4 in the absence of SO_2. Two peaks are readily observed, corresponding to the oxidation–reduction of metal and desorption–adsorption of hydrogen on the catalyst surface. The high potential peak shows the monolayer oxide formation-reduction of the catalyst layer in 30 wt% H_2SO_4 is observed. The low potential peak in the potential

region between 0.24 and 0.1 V vs. SHE corresponds to the hydrogen adsorption-desorption on the catalyst surface.

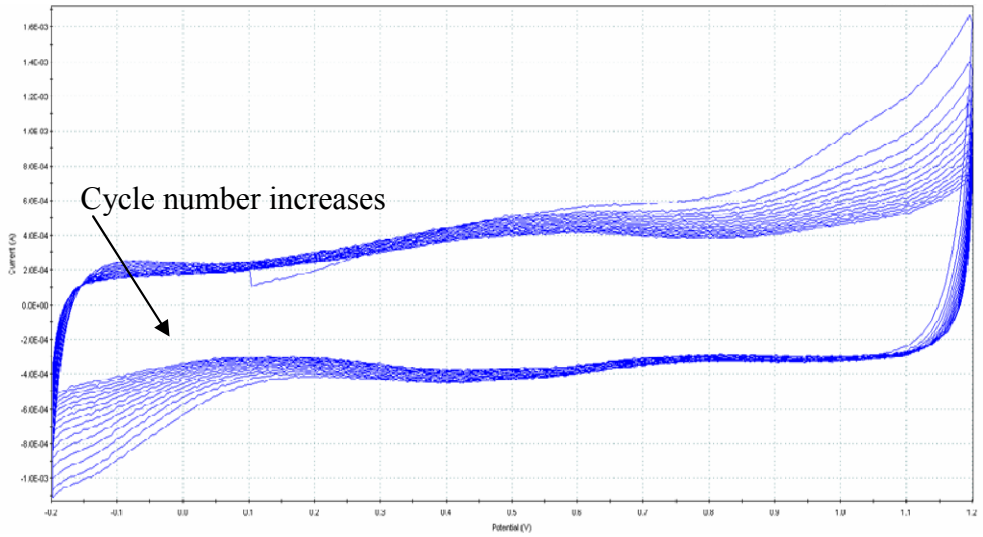

Figure 7. Typical cyclic voltammograms after consecutive cycling for Ru/C in 30 wt% H_2SO_4 purged with N_2 at room temperature.

In general, the area under the hydrogen adsorption-desorption peak gives an idea of the electrochemically active surface area available for reaction. The difference in the hydrogen desorption peak height after consecutive cycling can be observed in Figure 7. In the case of the Pt/C and the PtM/C (M=Co, Cr, Fe) catalyst, the peak tends to increases until it stabilizes, see Figure 8a. The initial increase could correspond to a combination of wetting by the electrolyte of the catalyst surface and activation of the catalyst surface. In the case of PtM/C (M=Ru, Ir) and Ru/C the surface area progressively decreases with each cycle, see Figure 8b.

A reduction in the peak area will indicate a reduction of active sites due to agglomeration of metal particles on the support, dissolution of metal in the electrolyte, or deactivation of active sites due to a poisoning agent.

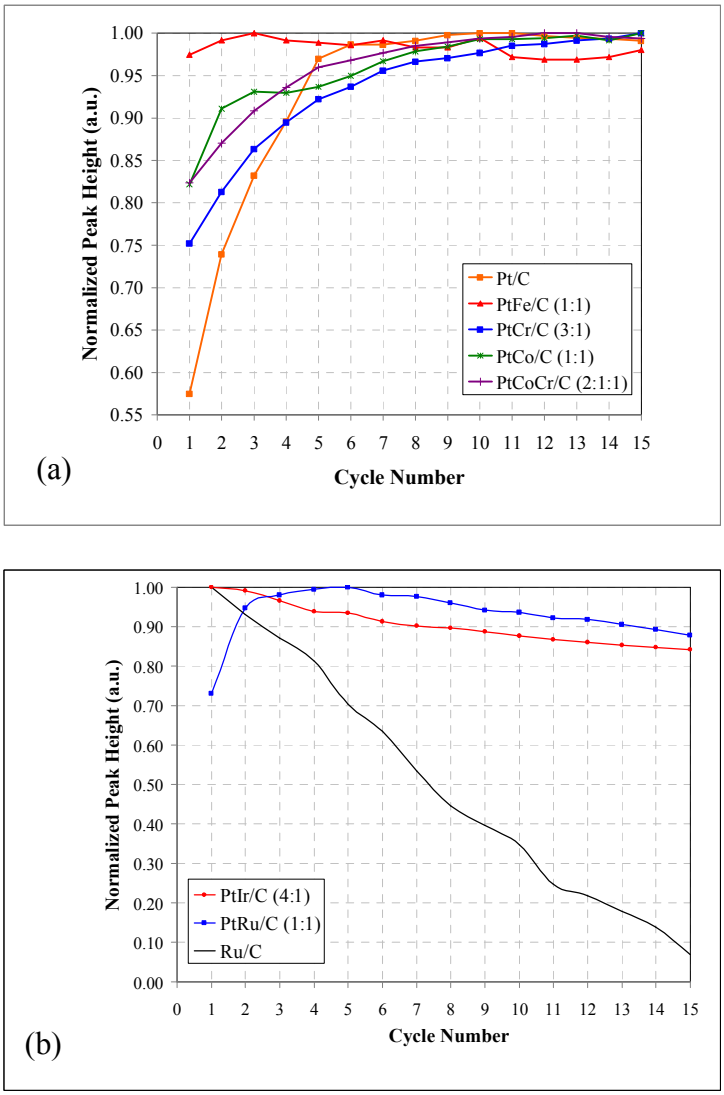

Figure 8. Normalized hydrogen desorption peak height after consecutive cycling for (a) Pt/C and PtM/C (M=Co, Cr, Fe) and (b) Ru/C and PtM/C (M=Ru, Ir) in 30 wt% H_2SO_4 purged with N_2 at room temperature.

4.4 ELECTROCATALYST ACTIVITY

Selecting the right catalyst will have an impact on the electrical efficiency by allowing the SDE to operate at conditions closer to the reversible potential. The electrocatalytic activity of the Pt base catalysts was investigated for the oxidation of SO_2 in 30 wt% sulfuric acid solutions at room temperature. The typical LSV is shown in Figure 9 in the form of Tafel plot as the catalyst is cycled. LSVs measuring SO_2 oxidation for platinum and all platinum alloys revealed this interesting trend. Subsequent LSVs showed a rapid decrease in equilibrium potential measurements on a per cycle basis. Initially the decrease in potential was pronounced. After multiple cycles, the drop in potential decreases until finally after 15 or more cycles the equilibrium potential stabilizes. The behavior indicates the possible activation of the catalyst surface, such as the formation of a layer of adsorbed sulfur species on the catalyst surface [17]. Figure 10 shows a summary of the initial open circuit potential (OCP) when the electrode is inserted in the fresh solution and after the electrode is cycled and an steady OCP is obtained. It is interesting to note that the best end OCP is observed when Pt is alloyed with non-noble metals such as cobalt, chromium or iron and the abundance of non-noble metal atoms is higher than Pt. However, when Pt is alloyed with noble metals such as iridium or ruthenium the OCP is similar to Pt or higher.

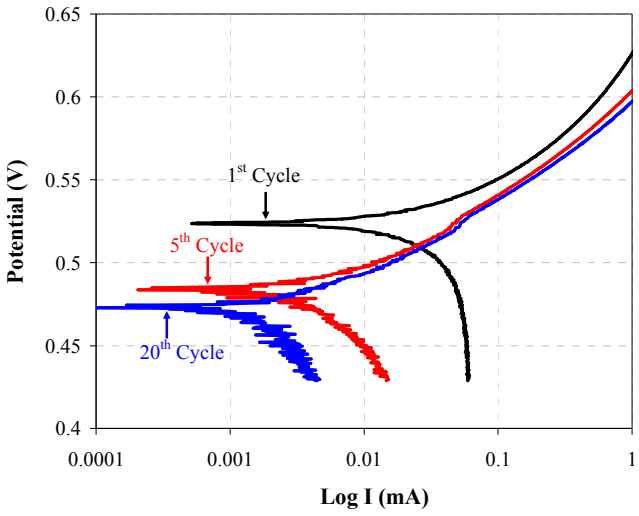

Figure 9. Typical Tafel plot for PtCr/C in 30 wt% sulfuric acid, saturated with SO_2 at room temperature. Three different potential cycles are shown.

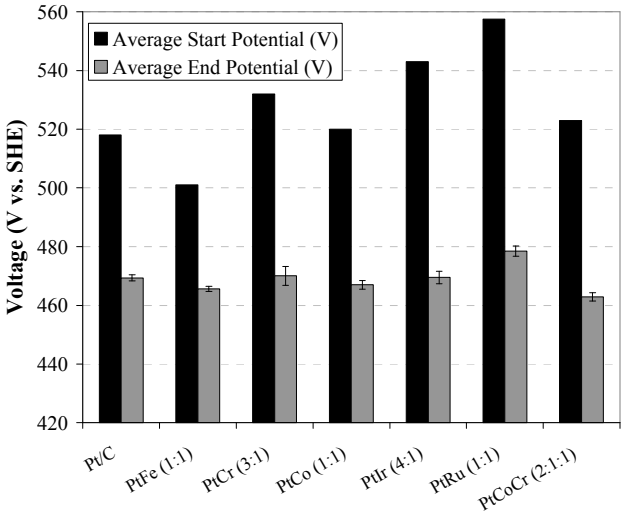

Figure 10. Open circuit potential for the different catalysts at the beginning of the test and after reaching near steady state conditions. Tested in 30 wt% sulfuric acid, saturated with SO_2 at room temperature.

5.0 CONCLUSIONS

Progress has been made in identifying PEMs that exhibit reduced transport of SO_2. Of the PFSA-type membranes, the Dupont bilayer, the 1500EW membrane, the two treated PFSA membranes from Dupont, and the PFSA-FEP blends from Case Western Reserve University all showed reduced SO_2 transport relative to the baseline membrane Nafion® 115. Of the non-PFSA membranes, BPVE and BPVE-6F from Clemson University, and the Celtec-V PBI membrane from BASF also showed reduced SO_2 transport. Only the BPVE, BPVE-6F, and PBI membranes exhibited increased electrolyzer performance coupled with lower SO_2 transport. The PBI membrane, Celtec-V, exhibited the best combination of performance and SO_2 transport, with a 27% increase in current density and a 67% decrease in SO_2 transport, compared to the baseline membrane Nafion® 115.

It should be noted that all of the non-PFSA type membranes tested were either designed for or should be capable of operating at higher temperatures (PBI < 200 °C, SDAPP < 285 °C, BPVE-6F > 100 °C) than that allowed in the current testing system (80 °C) all. Future work will involve testing at elevated temperatures (120 °C) and pressures. The increase in operating temperature is expected to decrease the kinetic overpotential loss thereby increasing the electrolyzer performance, for the high temperature membranes, SDAPP, BPVE-6F, and PBI.

The stability and activity of anode and cathode catalysts at 30 wt% acid concentration was studied on commercially available catalysts. It is desired for the SDE to have catalysts with high chemical and electrochemical stability. Among the catalysts tested Pt/C and PtM/C (M=Co, Cr, Fe) showed good stability, while catalysts containing Ir or Ru showed degradation as a function of cycling. The SO2 oxidation activity of the different catalysts was improved for catalysts with higher atomic concentration of non-noble metals such as cobalt, chromium or iron than Pt. However, when Pt is alloyed with noble metals such as iridium or ruthenium the OCP is similar to Pt or higher.

6.0 REFERENCES

1. J. Udagawa, P. Aguiar, N. P. Brandon. Journal of Power Sources. 166 (2007) 127.
2. J. E. Funk. International Journal of Hydrogen Energy. 26 (2001) 185.
3. M. B. Gorensek, J. A. Staser, T. G. Stanford, J. W. Weidner. International Journal of Hydrogen Energy, 34 (2009) 6089-6095.
4. Westinghouse Electric Corporation, A Study on the Electrolysis of Sulfur Dioxide and Water for the Sulfur Cycle Hydrogen Production Process, AESD-TME-3043, July 1980.
5. J. L. Steimke, T. J. Steeper, Characterization Testing of H_2O-SO_2 Electrolyzer at Ambient Pressure, Westinghouse Savannah River Company, Technical Report WSRC-TR-2005-00310, August 1, 2005.
6. J. L. Steimke, T. J. Steeper, Characterization Testing and Analysis of Single Cell SO2 Depolarized Electrolyzer, Washington Savannah River Company, Technical Report WSRC-STI-2006-00120, September 15, 2006.
7. K. A. Mauritz, R. B. Moore. Chem. Rev. 104 (2004) 4535-4585.
8. L. Xiao, H. Zhang, E. Scanlon, L. S. Ramanathan, E. Choe, D. Rogers, T. Apple, B. C. Benicewicz. Chem. Mater. 17 (2005) 5328-5333.
9. C. H. Fujimoto, M. A. Hickner, C. J. Cornelius, D. A. Loy. Macromolecules. 38 (2005) 5010-5016.
10. J. Jin, J. Stanbro, D. Van Derveer, D. W. Smith. PMSE Preprints. 91 (2004) 504-505.
11. R. Bouchet, E. Siebert. Solid State Ionics 118 (1999) 287–299.
12. X. Glipa, B. Bonnet, B. Mula, D. J. Jones, J. RozieÁre, J. Mater. Chem. 9 (1999) 3045-3049.
13. K. A. Perry, G. A. Eisman, B. C. Benicewicz. Journal of Power Sources. 177 (2008) 478-484.
14. C. B. Shogbon, J. Brousseau, H. Zhang, B. C. Benicewicz, Y. A. Akpalu. Macromolecules. 39 (2006) 9409-9418.
15. J. L. Steimke, T. J. Steeper, D. T. Herman, H. R. Colon-Mercado, M. C. Elvington. Savannah River Nuclear Solutions, Technical Report SRNS-STI-2009-00134, September 15, 2006.
16. A. Shaver, H. Boily, A. Lebuis. Inorganic Chemistry. 35 (1996) 6356-6357.

17. C. Quijada, J. L. Vazques, A. Aldaz. Journal of Electroanalytical Chemistry. 414 (1996) 229-233.